

Particle-in-Cell Simulation of the Measurement of Laser Wakefields with Raman Scattering of Probe Laser Light

Weimin ZHOU, Kunioki MIMA and Hideo NAGATOMO

Institute of Laser Engineering, Osaka University, Suita, Osaka 565-0871, Japan

(Received 24 September 2008 / Accepted 11 November 2008)

A diagnostic method for measuring nonlinear evolution of a laser wakefield by multiple sidebands of Raman scattering using probe laser light has been reported. In this paper, particle-in-cell simulations are used to demonstrate the validity of this probing method. The influence of plasma density, pump laser intensity, propagation length, and nonlinearity of the wakefield on probe laser light has been investigated. In particular, when trapping and acceleration of electrons occurs, the wing structure of the spectrum of probe laser light indicates the existence of highly relativistic electrons from which the injection fraction of the accelerated electrons can be obtained. Thus, this diagnostic method can be employed to measure laser wakefields conveniently for various purposes.

© 2008 The Japan Society of Plasma Science and Nuclear Fusion Research

Keywords: intense laser, wakefield, Raman scattering, probe laser light, particle-in-cell simulation

DOI: 10.1585/pfr.3.063

1. Introduction

Since first suggested by Tajima and Dawson [1] about three decades ago, laser wakefield acceleration (LWFA) has been studied in theory [2–7], simulation [8–10], and experiment [11–13] because of its promising applications using the principles of physics. In LWFA, when an intense and short laser pulse is injected into an underdense plasma, the laser ponderomotive force expels electrons longitudinally. Since the velocity of electrons is always lower than that of light in the underdense plasma, after the pump laser pulse passes, large amplitude plasma waves of strong charge-separation electric fields called wakefields are generated. The phase velocity of the wakefields equals the laser group velocity in the underdense plasma.

The most promising application of LWFA is the laser plasma accelerator. Due to the large amplitude electric fields related to wakefields, electrons with sufficient energy that matches the phase of the accelerating fields can be trapped and accelerated to highly relativistic energy of the order of hundreds of MeV. For the electrons to be trapped and accelerated, they need to be injected into the wakefield with sufficient energy and match the accelerating phase precisely. Several injection schemes have been proposed [7, 9, 14–16] and demonstrated in experiments [11–13, 17–24] successfully. These injection schemes can be classified as extra-injection, using two or three colliding laser beams [14, 15, 20]; and self-injection, which consists of a self-modulated LWFA (SMLWFA) [7, 11, 12, 17, 18], wave breaking injection [9, 13], and beam loading in the bubble regime [16, 19, 21–24].

To measure the amplitude of laser wakefields, a vari-

ety of known diagnostic methods employ techniques such as frequency-domain interferometry [25, 26], photon acceleration [27], and coherent Thomson scattering [28–30]. For the diagnosis of electron injection into a wakefield, it is reported that tremendous broadening of anti-Stokes peaks of the pump laser is characteristic of wave breaking, because coherence is lost as the wave breaks [11]. The observation of spatially localized broadband radiation emission perpendicular to the direction of propagation of pump laser has been presented to correlate the production of beams of relativistic electrons [31]. However, there have been no reports on quantitative measurement of the fraction of electron injection.

Recently, a scheme for measuring nonlinear evolution of a laser wakefield by multiple sidebands of forward Raman scattering of probe laser light was presented [32]. In this scheme, a relatively long and weak probe laser pulse is injected into the wake behind the pump laser. As the amplitude of the probe laser is very small compared with that of the pump laser, it does not influence the wakefield; however, probe laser light is modulated by the density fluctuation associated with the wakefield. From the wave equation describing the propagation of probe laser light in the wake, an analytical solution for the multiple sidebands is given [32] by

$$b(\omega_0 + l\omega_p) = \frac{\omega_p^2 N(l)b(\omega_0)L_g}{2(\omega_0 + l\omega_p)v_g}, \quad (1)$$

where $b(\omega_0 + l\omega_p)$ and $b(\omega_0)$ are the amplitudes of the l th sideband at $\omega_0 + l\omega_p$ and the fundamental component at ω_0 of the scattered probe laser light after propagating a distance of L_g with group velocity v_g , respectively; ω_0 is the fundamental frequency of probe laser light;

author's e-mail: zhouwm@ile.osaka-u.ac.jp

$\omega_p = \sqrt{4\pi e^2 n_0 / m_e}$ is the electron plasma frequency; $N(l)$ is the amplitude of the l th harmonic of the plasma wave $\delta(n_e/n_0\gamma) = n_e/n_0\gamma - 1$, n_e ; γ is the local electron density and relativistic factor; and n_0 is the initial plasma density. This analytical solution indicates that the sideband amplitude of scattered probe laser light is proportional to the ambient plasma density, the propagation distance of the probe laser, and the amplitude of the corresponding plasma wave. In the experiment, if the Raman sidebands spectra are obtained, the amplitude of the wakefield can be determined.

In this paper, we have described a series of PIC simulations that were performed to investigate the validity of this scheme. The influence of the initial plasma density, the amplitude of the pump laser, and the propagation length of the probe light is studied. It is found that this scheme is appropriate for a wide range of laser wakefield measurements. Moreover, we simulated some cases with electron injection. The influence of trapped and accelerated electrons is shown in the spectrum of probe laser light. The wing structure in the spectrum of probe laser light indicates the existence of the accelerated relativistic electrons, and we can obtain the electron injection fraction quantitatively.

2. PIC Simulations

For these simulations, since both the excitation of the wakefield and Raman scattering are one-dimensional (1D) effects, 1D fully electromagnetic PIC code is used. In the simulations, the total length is $500\lambda_0$, the cell size is $0.05\lambda_0$, and the time step is $0.05\tau_0$, where λ_0 and τ_0 are the wavelength and the period, respectively, of the pump laser. A homogeneous plasma having a length of $L_g = 200\lambda_0$ - $400\lambda_0$ is located at the center of a simulation box. In each cell, 20 simulation particles representing electrons are placed, and ions are fixed as an immobile background. For typical laser wakefield acceleration, the plasma density $n_e = 10^{18}$ - 10^{19} cm^{-3} . The critical plasma density $n_c = 1.1 \times 10^{21} \text{ cm}^{-3}$ for $\lambda_0 = 1 \mu\text{m}$. Therefore, in the simulations, we set the plasma density as $2.5 \times 10^{-3}n_c$ - $1.0 \times 10^{-2}n_c$ so that it corresponds to the typical laser wakefield cases. The incident pump laser is linearly polarized, and has a longitudinal profile $a = a_0 \sin(\pi x/L)$, where $a_0 = \sqrt{I\lambda_0^2/1.38 \times 10^{18}}$ is the normalized vector potential, and L is the laser length. The laser intensity required to generate the laser wakefield is of the order of 10^{18} W/cm^2 . Therefore, the normalized vector potential used in the simulations has the range $a_0 = 0.5$ - 2.2 . For maximal wakefield excitation, the laser length must equal the plasma wavelength ($L \approx \lambda_p$) [2]. In the simulations, the laser lengths are set to satisfy this requirement for various plasma densities. For diagnosing the wakefield, a probe laser pulse is injected behind the pump laser. The probe laser pulse has the same polarization as the pump laser; however, the frequency of the probe laser is doubled to make the spectral measurement in experiments easier and solution (1) valid

longer. Probe laser light has a relatively long length and weak intensity compared with that of the pump laser. Thus, in the longitudinal space, the probe laser rises in $10\lambda_0$, maintains its peak amplitude $b_0 = 0.05$ for $80\lambda_0$, and then falls in $10\lambda_0$. In this scheme, the location of the probe laser does not require precise control compared with other schemes. In all simulations, the interval between the pump laser and the probe laser is fixed as $10\lambda_0$.

In the first series of simulations, the plasma length is fixed as $L_g = 300\lambda_0$, but the densities are varied as follows: $2.5 \times 10^{-3}n_c$, $6.4 \times 10^{-3}n_c$, and $1.0 \times 10^{-2}n_c$, corresponding to plasma wavelengths of $20\lambda_0$, $12.5\lambda_0$, and $10\lambda_0$. Therefore, pump laser lengths are adjusted to the corresponding values, but the intensities are all maintained at $a_0 = 0.8$. Figure 1 plots the profiles and spectra of the plasma oscillation $\delta(n_e/n_0\gamma)$ in the first series till the pump lasers reach $280\lambda_0$. This shows that the wakefield wavelengths correspond well with the expectation $k_p = \sqrt{4\pi e^2 n_0 / m_e c^2}$. In the first series, the pump laser intensities are the same. From nonlinear plasma theory, it is derived that the wakefield amplitude is correlated to the pump laser intensity. Therefore, the wakefield amplitudes in the first series are constant, as shown in Fig. 1.

Figure 2 shows the spectra of probe laser light after propagating through $300\lambda_0$. As expected from Eq. (1), multiple sidebands appear around the fundamental frequency. The frequency shift between the l th sideband and the fundamental is $l\omega_p$. The amplitudes of the first up-shifted anti-Stokes and down-shifted Stokes are the strongest, because they represent the fundamental components of the wakefields; however, signals of the second and third sidebands are also observed. Amplitudes of both the wakefield and scattered probe laser light are proportional to the plasma frequency. Thus, comparison of the three

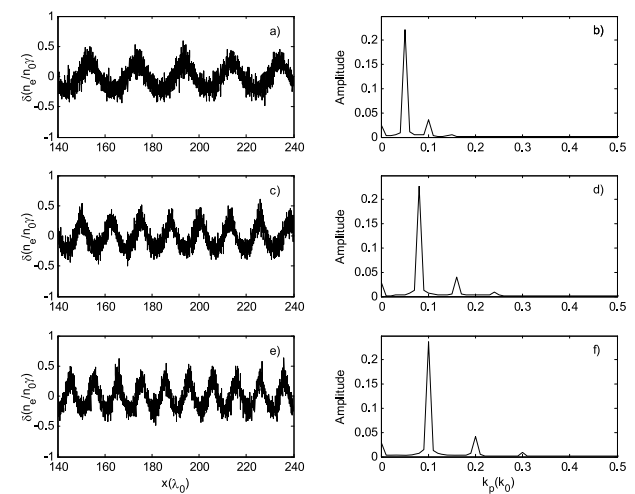


Fig. 1 Profiles and spectra of plasma oscillation when the pump lasers reach $280\lambda_0$ for a pump laser of $a_0 = 0.8$, with plasma density a) and b) $n_e = 2.5 \times 10^{-3}n_c$, c) and d) $n_e = 6.4 \times 10^{-3}n_c$, e) and f) $n_e = 1.0 \times 10^{-2}n_c$.

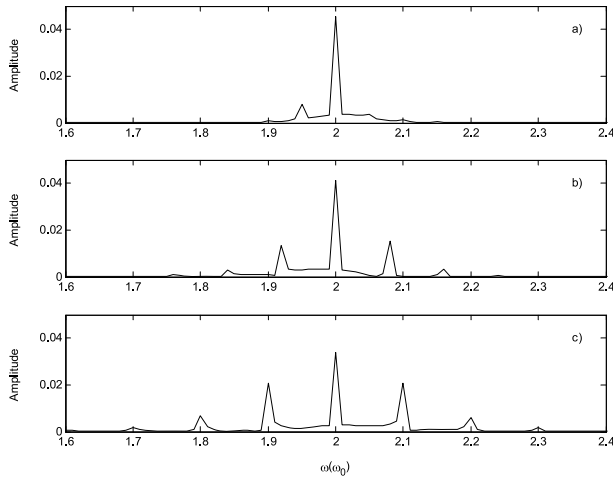


Fig. 2 Spectra of probe laser lights after co-propagation with a wakefield of $300\lambda_0$ for a pump laser of $a_0 = 0.8$, with plasma density a) $n_e = 2.5 \times 10^{-3} n_c$, b) $n_e = 6.4 \times 10^{-3} n_c$, c) $n_e = 1.0 \times 10^{-2} n_c$.

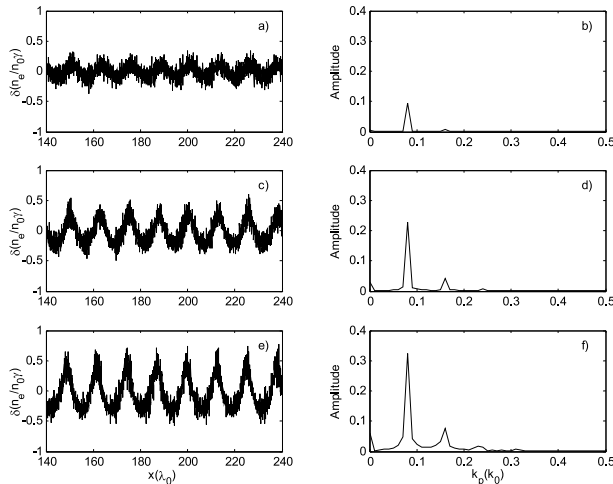


Fig. 3 Profiles and spectra of plasma oscillation when the pump lasers reach $280\lambda_0$ for a plasma density of $n_e = 6.4 \times 10^{-3} n_c$, with pump laser a) and b) $a_0 = 0.5$, c) and d) $a_0 = 0.8$, e) and f) $a_0 = 1.0$.

cases in the first series shows that the sideband amplitudes are higher for plasma with higher density and frequency.

In the second series of simulations, the plasma density is fixed as $6.4 \times 10^{-3} n_c$; the pulse width of the pump lasers is fixed as $L = 12.5\lambda_0$, but the pump laser intensities are varied as $a_0 = 0.5, 0.8$ and 1.0 . The profile and spectrum of the wakefield for $a_0 = 0.5$, as shown in Fig. 3 a), indicate that the wakefield is monochromatic with wavelength k_p . Therefore, only the first anti-Stokes and Stokes are observed in the spectrum of the probe laser, as shown in Fig. 4 a).

When pump laser strength increases sufficiently to be relativistic ($a_0 \sim 1.0$), relativistic nonlinear effects become important. Then, the waveform of the wakefield steepens,

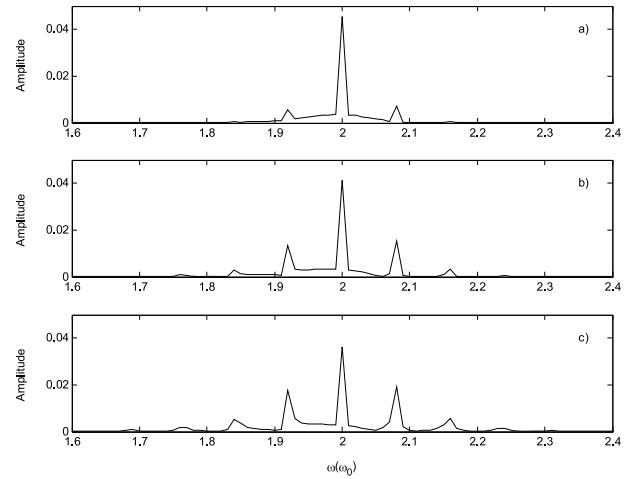


Fig. 4 Spectra of probe laser lights after co-propagating with a wakefield of $300\lambda_0$ for a plasma density of $n_e = 6.4 \times 10^{-3} n_c$, with pump laser a) $a_0 = 0.5$, b) $a_0 = 0.8$, and c) $a_0 = 1.0$.

which corresponds to the generation of high harmonics in its spectrum [3]. These phenomena are observed in the profiles and spectra of the wakefield for $a_0 = 0.8$ and 1.0 (Figs. 3 b)–f)). It is shown that for higher pump laser intensity, the wakefield amplitudes are higher, because the wakefield amplitude is proportional to the pump laser intensity. Spectra of the probe laser light in this series are plotted in Fig. 4. The relation between the sideband amplitudes of probe laser light and the wakefield spectrum agrees well with that predicted by Eq. (1).

Since the sideband amplitude of the scattered probe laser is proportional to the propagation distance, in the third series of simulations, we maintain $n_e = 6.4 \times 10^{-3} n_c$, $L = 12.5\lambda_0$, and $a_0 = 0.8$, and then measure the probe laser after propagating through $L_g = 200\lambda_0, 300\lambda_0$, and $400\lambda_0$. The spectra of the probe laser measured at the different propagation distances are shown in Fig. 5, and agree well with those obtained using Eq. (1).

Therefore, when the spectrum of the probe laser is measured, the plasma wakefield amplitude and the structure factor can be determined from Eq. (1). All parameters in the above three series of simulations are plotted in Table 1. $b(2\omega_0)$ and $b(2\omega_0 + \omega_p)$ are the amplitudes of the fundamental component and first sideband of probe laser light. Substituting these parameters into Eq. (1), the amplitude of the fundamental component of the wakefield $N_1(\omega_p)$ is obtained using Eq. (1). $N_2(\omega_p)$ is the amplitude of the fundamental component of the wakefield measured directly in the PIC simulation. The maximum error of these two values is 11.9%. It can be concluded that this probing method is applicable to measuring the laser wakefield structure from the laser scattering data. Data of higher harmonics are not listed in the table; however, it was ascertained that they agree well with the predicted values ob-

tained using Eq. (1).

It is widely accepted that the most promising application of LWF is the laser accelerator. To determine the influence of trapped and accelerated electrons on probe laser light, we simulated a series of cases in which electrons are well trapped and accelerated by wakefields using different injection schemes. In this series, the probe laser parameters are the same as in the previous series, but the pump laser and plasma densities are changed for every case, according to the corresponding injection scheme.

First, we simulate a case without trapping and accelerating the electrons. In this case, the plasma density is $6.4 \times 10^{-3}n_c$ and the length of the plasma region is $400\lambda_0$. The pump laser amplitude is $a_0 = 1.2$, and the pulse width is $L = 12.5\lambda_0$. The electron distribution in $p_x - x$ phase space when the front of the pump laser arrives at $x = 440\lambda_0$ is plotted in Fig. 6 a), which shows that there are no electrons injected and trapped, although wave breaking nearly occurs. The corresponding spectrum of probe laser light is shown in Fig. 7 a).

In the second case, extra injection via two colliding laser pulses [14,15,20] is simulated. The plasma and pump

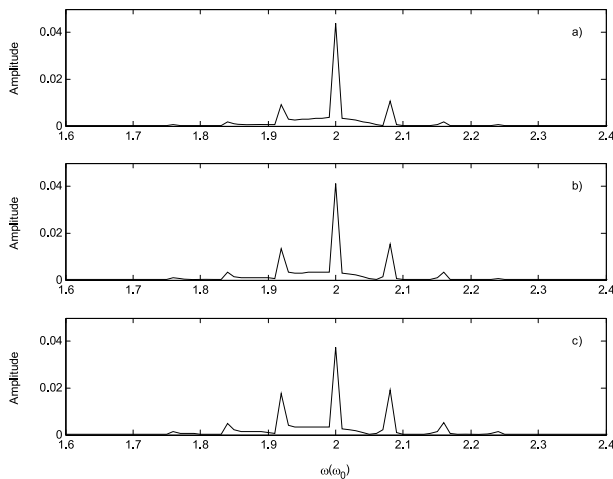


Fig. 5 Spectra of probe laser light for a pump laser of $a_0 = 0.8$ with a plasma density of $n_e = 6.4 \times 10^{-3}n_c$ after co-propagating with a wakefield of a) $L_g = 200\lambda_0$, b) $L_g = 300\lambda_0$ and c) $L_g = 400\lambda_0$.

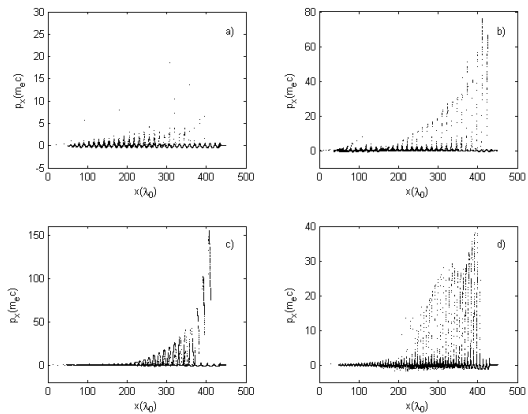


Fig. 6 Electron distributions in phase space for schemes a) without electron injection, b) with electron injection via colliding lasers, c) with electron injection via wave breaking, and d) with electron injection via SMLWFA.

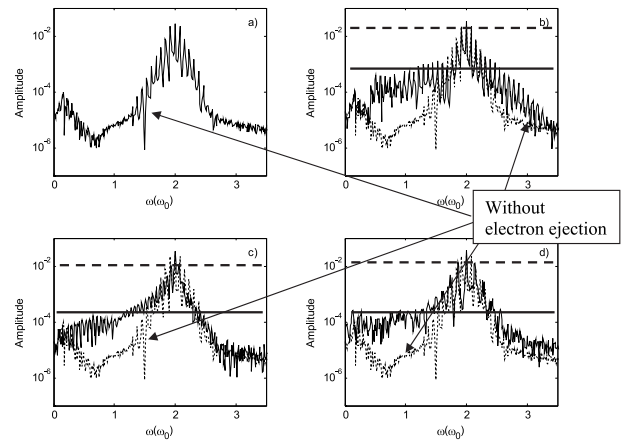


Fig. 7 a) Spectrum of probe laser light for the scheme without electron injection; b) spectrum (solid line) for the scheme with electron injection via colliding lasers; c) with electron injection via wave breaking; and, d) with electron injection via SMLWFA. The dotted line represents no electron injection. Amplitude of first harmonic (bold solid line), and wing structure (bold dashed line).

Table 1 Parameters and results of PIC simulations.

a_0	0.8	0.8	0.8	0.5	1.0	0.8	0.8
$n_0(n_c)$	0.0025	0.0064	0.01	0.0064	0.0064	0.0064	0.0064
$b(2\omega_0)$	0.0456	0.0413	0.034	0.0455	0.0363	0.0441	0.0374
$b(2\omega_0 + \omega_p)$	0.0058	0.0144	0.0206	0.0063	0.0185	0.0098	0.0185
$L_g(\mu m)$	300.0	300.0	300.0	300.0	300.0	200.0	400.0
$v_g(c)$	0.9994	0.9984	0.9975	0.9984	0.9984	0.9984	0.9984
$N_1(\omega_p)$	0.2228	0.2395	0.2699	0.0951	0.3505	0.2299	0.2552
$N_2(\omega_p)$	0.2219	0.2269	0.2395	0.0959	0.3169	0.2269	0.2269
Error (%)	0.4	5.4	11.9	0.9	10.0	1.3	11.7

laser parameters are the same as in the earlier case. In addition to the pump laser, there is a counter-propagating laser pulse with the same frequency, polarization, and length of the pump laser. The amplitude of the counter laser is 0.4. The two laser pulses collide at $x = 100\lambda_0$ and the colliding laser pulse injects electrons into the wakefield. In the third simulation, the plasma parameters are the same as in the previous case, but the pump laser amplitude is increased to $a_0 = 2.2$. In this highly relativistic intensity regime, the seed electrons can be self-injected into the wakefield by wave breaking [9, 13]. This is called self-injection WFA (SIWFA). The last case of this series is the simulation of the injection scheme via SMLWFA [7, 11, 12, 17, 18]. In this scheme, the plasma density is higher than the plasma density satisfying $\lambda_p \approx L$. Thus, the plasma density in this case is adjusted to $2.0 \times 10^{-2}n_c$, and other parameters are the same as in the first case of this series.

Electron distributions in the $p_x - x$ phase space for the last three cases are plotted in Figs. 6 b)–d). We can see that these schemes are efficient for trapping and accelerating electrons. Comparison of Fig. 7 a) with Figs. 7 b), c), d) shows wide wings in the spectrum of the scattered probe laser. In the case where electrons are trapped and accelerated, the plasma density $N(l) = N_p(l) + N_b(l)$, where $N_b(l)$ is the distribution from trapped and accelerated bunch electrons, and $N_p(l)$ is the distribution of the background electron plasma wave. These wings correspond to laser scattering by narrow electron bunches, namely, the contribution of $N_b(l)$. The wing formation is similar in the spectrum of the pump laser, because of stimulated Raman scattering when wave breaking occurs [11]. In our paper, the wing structure of probe light is due to electrons trapped and accelerated by the wakefield.

Figure 8 shows that the width of the wing ($\Delta\omega_b$) is inversely proportional to the bunch width in one wakefield potential well (L_b) because $L_b = 2\pi c/\Delta\omega_b$. Since the wing extends to $\pm 20\omega_p$, the bunch width can be determined as $\omega_p/20$ from the spectrum. On the other hand, the width of each sideband ($\Delta\omega_a$) is inversely proportional to the length where effective trapping and acceleration occur (L_a) as $L_a = 2\pi c/\Delta\omega_a$. Here, the width of sideband is about $\lambda_p/10$, so the effective accelerating length can be determined as $10\lambda_p$.

The wing structures differ between Fig. 7 b), and Figs. 7 c) and d). One difference is that the relative amplitude of the wing (the solid horizontal line) to the first harmonic (broken horizontal line) is higher for counter laser injection (Fig. 7 b). Moreover, the relative amplitude is two times the magnitude when compared with the other two schemes (Figs. 7 c) and d)). This indicates that the number of injected electrons relative to the wakefield density fluctuation for counter laser injection is two times higher than those for the other cases. As a consequence, Eq. (1) can be used to determine the total bunch electron charge from the scattered laser spectrum.

Each sideband spectrum in the wing shown in Fig. 7 b)

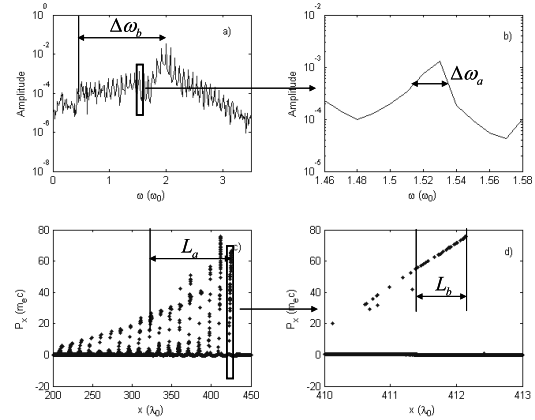


Fig. 8 a) Spectrum of probe laser light; b) a close up of the square in a); c) the electron distribution in phase space; and, d) a close up of the square in c) with electron injection via colliding lasers.

is narrower than those in Figs. 7 c) and d). This indicates that the number of bunch electrons is greater for the counter laser injection than for the SIWFA. When the linewidth of one sideband line is $\Delta\omega$, the number of bunches is estimated to be $\omega_p/\Delta\omega$.

3. Conclusion

The Raman scattering formula, Eq. (1) and the 1D PIC simulations validate the diagnostic scheme of measuring the nonlinear evolution of a laser wakefield and the trapped electrons by the higher order sidebands of Raman scattering of probe laser light. The results of PIC simulations imply that this diagnostic scheme can be employed to measure a laser wakefield for a large parameter range of plasma density, plasma length, and pump laser amplitude. In particular, it was found that the wing structure in the scattered probe laser spectrum is useful for diagnosing the trapping and acceleration of electron bunches. It was also found that the number of bunches depends on the trapping process. Moreover, the number of bunches is significantly large for counter propagation laser injection. In the future, the 2- and 3-dimensional diagnostics of the wakefield structure and the trapped electron bunch structure will be investigated.

Acknowledgments

This work was supported by MEXT, a Grant-in-Aid for Creative Scientific Research (15GS0214), and by an aid from the Computation Group at ILE.

- [1] T. Tajima and J.M. Dawson, Phys. Rev. Lett. **43**, 267 (1979).
- [2] P. Sprangle, E. Esarey, A. Ting and G. Joyce, Appl. Phys. Lett. **53**, 2146 (1988).

- [3] P. Sprangle, E. Esarey and A. Ting, *Phys. Rev. Lett.* **64**, 2011 (1990).
- [4] P. Sprangle, E. Esarey, J. Krall and G. Joyce, *Phys. Rev. Lett.* **69**, 2200 (1992).
- [5] T.M. Antonsen and P. Mora, *Phys. Rev. Lett.* **69**, 2204 (1992).
- [6] E. Esarey, J. Krall and P. Sprangle, *Phys. Rev. Lett.* **72**, 2887 (1994).
- [7] E. Esarey, B. Hafizi, R. Hubbard and A. Ting, *Phys. Rev. Lett.* **80**, 5552 (1998).
- [8] W.B. Mori, C. Joshi and J.M. Dawson, *Phys. Rev. Lett.* **60**, 1298 (1988).
- [9] K.-C. Tzeng, W.B. Mori and T. Katsouleas, *Phys. Rev. Lett.* **79**, 5258 (1997).
- [10] F.S. Tsung, R. Narang, W.B. Mori, C. Joshi, R.A. Fonseca and L.O. Silva, *Phys. Rev. Lett.* **93**, 185002 (2004).
- [11] A. Modena, Z. Najmudin, A.E. Dangor *et al.*, *Nature (London)* **377**, 606 (1995).
- [12] D. Umstadter, S.-Y. Chen, A. Maksimchuk, G. Mourou and R. Wagner, *Science* **273**, 472 (1996).
- [13] V. Malka, S. Fritzler, E. Lefebvre *et al.*, *Science* **298**, 1596 (2002).
- [14] D. Umstadter, J.K. Kim and E. Dodd, *Phys. Rev. Lett.* **76**, 2073 (1996).
- [15] E. Esarey, R.F. Hubbard, W.P. Leemans, A. Ting and P. Sprangle, *Phys. Rev. Lett.* **79**, 2682 (1997).
- [16] A. Pukhov and J. Meyer-ter-Vehn, *Appl. Phys. B* **74**, 355 (2002).
- [17] K. Nakajima, D. Fisher, T. Kawakubo *et al.*, *Phys. Rev. Lett.* **74**, 4428 (1995).
- [18] C.A. Coverdale, C.B. Darrow, C.D. Decker *et al.*, *Phys. Rev. Lett.* **74**, 4659 (1995).
- [19] C.I. Moore, A. Ting, K. Krushelnick, E. Esarey, R.F. Hubbard, B. Hafizi, H.R. Burris, C. Manka and P. Sprangle, *Phys. Rev. Lett.* **79**, 3909 (1997).
- [20] J. Faure, C. Rechatin, A. Norlin, A. Lifschitz, Y. Glinec and V. Malka, *Nature (London)* **444**, 737 (2006).
- [21] S.P. Mangles, C.D. Murphy, Z. Najmudin *et al.*, *Nature (London)* **431**, 535 (2004).
- [22] C.G.R. Geddes, Cs. Toth, J. van Tilborg *et al.*, *Nature (London)* **431**, 538 (2004).
- [23] J. Faure, Y. Glinec, A. Pukhov *et al.*, *Nature (London)* **431**, 541 (2004).
- [24] C.-L. Chang, C.-T. Hsieh, Y.-C. Ho *et al.*, *Phys. Rev. E* **75**, 036402 (2007).
- [25] J.R. Marquès, J.P. Geindre, F. Amiranoff, P. Audebert, J.C. Gauthier, A. Antonetti and G. Grillon, *Phys. Rev. Lett.* **76**, 3566 (1996).
- [26] S.C. Siders, S.P. Le Blanc, D. Fisher, T. Tajima and M.C. Downer, *Phys. Rev. Lett.* **76**, 3570 (1996).
- [27] J.M. Dias, L. Oliveira e Silva and J.T. Mendonça, *Phys. Rev. ST Accel. Beams* **1**, 031301 (1998).
- [28] R.E. Slusher and C.M. Surko, *Phys. Fluids* **23**, 472 (1980).
- [29] A. Ting, K. Krushelnick, C.I. Moore *et al.*, *Phys. Rev. Lett.* **77**, 5377 (1996).
- [30] S.P. Le Blanc, M.C. Downer, R. Wagner *et al.*, *Phys. Rev. Lett.* **77**, 5381 (1996).
- [31] A.G.R. Thomson, S.P.D. Mangles, Z. Najmudin, M.C. Kaluza, C.D. Murphy and K. Krushelnick, *Phys. Rev. Lett.* **98**, 054802 (2007).
- [32] W. Zhou, K. Mima, T. Nakamura and H. Nagatomo, *Phys. Plasmas* **15**, 093107 (2008).